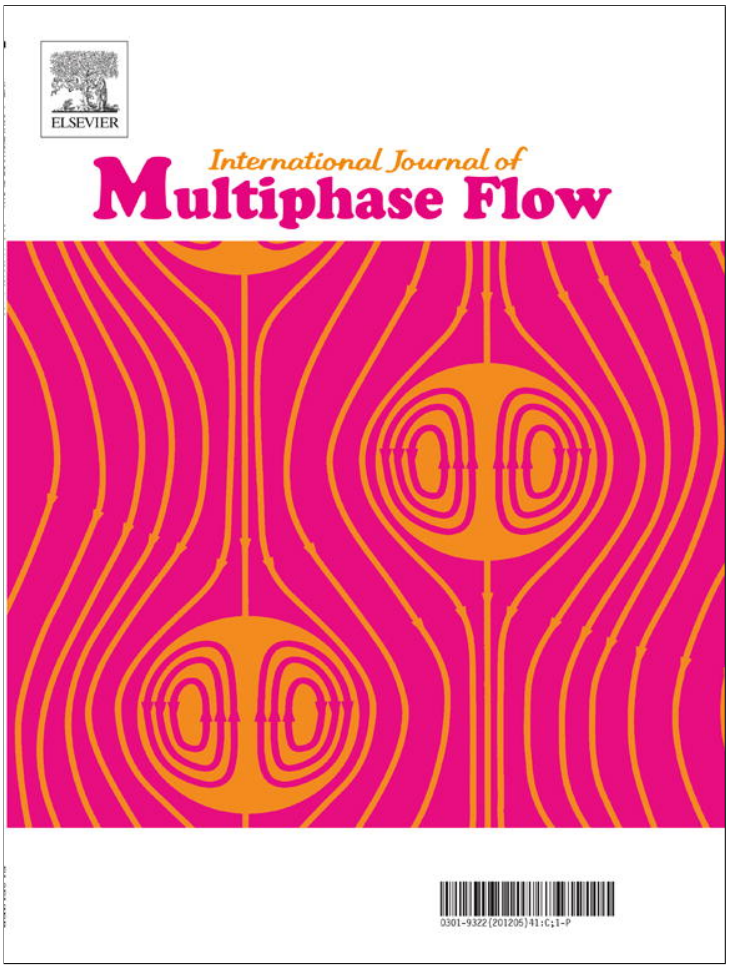

(This is a sample cover image for this issue. The actual cover is not yet available at this time.)

International Journal of Multiphase Flow 45 (2012) 12–23

Contents lists available at SciVerse ScienceDirect

International Journal of Multiphase Flow

journal homepage: www.elsevier.com/locate/ijmulflow

Flow pattern modulation in a horizontal tube by the passive phase separation concept

Hongxia Chen [a], Jinliang Xu [a,b,*], Zijin Li [b], Feng Xing [c], Jian Xie [c], Wei Wang [c], Wei Zhang [c]

[a] State Key Laboratory of Alternate Electrical Power System with Renewable Energy Sources, North China Electric Power University, Beijing 102206, China
[b] The Beijing Key Laboratory of New and Renewable Energy, North China Electric Power University, Beijing 102206, China
[c] The Beijing Key Laboratory of Multiphase Flow and Heat Transfer, North China Electric Power University, Beijing 102206, China

ARTICLE INFO

Article history:
Received 12 January 2012
Received in revised form 2 April 2012
Accepted 30 April 2012
Available online 12 May 2012

Keywords:
Condensation heat transfer
Phase separation
Mesh cylinder
Flow pattern modulation

ABSTRACT

A passive phase separation concept was proposed to modulate flow pattern in a condenser tube. An empty mesh cylinder is suspended in the condenser tube. The miniature mesh pores prevent gas bubble entering the mesh cylinder but capture liquid into the mesh cylinder, ensuring largest possibility for cold tube wall directly contacted with gas to form the perfect thin liquid film condensation heat transfer. We performed the air–water two-phase flow experiment. It was found that for a relatively higher liquid height in the horizontal tube, all liquid can be captured by the mesh cylinder to form the "gas-floating-liquid" mode. If the liquid height is small in the horizontal tube, partial liquid can be sucked by the mesh cylinder, the contact area between tube wall and gas is increased. When plug flow reaches the mesh cylinder surface, elongated saddle bubbles are formed in the annular region to envelop the mesh cylinder surface. When bubbly flow in the horizontal tube approaches the mesh cylinder area, miniature bubbles can merge to form large bubbles in the annular region. For the later two cases, all the gas flow rate is flowing in the annular region and the inside mesh cylinder is the liquid.

1. Introduction

The condensation heat transfer occurs in many industry applications such as air-conditioning, refrigeration, automotive and process industries. Increasing the condenser efficiency in these applications saves space and material and limits the refrigerant load. Higher efficiencies of these systems also reduce the running cost and environmental impact.

Recently, the low grade energy utilization has been received great attention due to the energy and environment problem. An efficient Organic Rankine Cycle (ORC) is a good solution to convert the low grade thermal energy ($T < 300$ °C) into electricity (David and Neil, 2010). In addition to search a better thermodynamic cycle and organic working fluids, a high condenser performance is also required. Under the operation condition of an ORC, the temperature difference between the organic fluid and the environment coolant (air or water) for the condenser should be small to ensure a large turbine power output. This requires a large heat transfer area of the condenser, increasing its fabrication cost. Besides, the condenser performance is quite sensitive to the dynamic variation of the coolant flow rate and temperature. The condenser performance should be good enough to ensure full condensation of fine bubbles of the organic fluid. Otherwise, the gas-corruption phenomenon is significant if the fine gas bubbles are attacking the rotating blades of the organic pump, shortening the pump lifetime.

Even though extensive studies have been performed on the condensation heat transfer in the past century, it is a long way to fully understand the complicated mechanism. In fact, the condensation heat transfer is strongly related to the vapor–liquid phase distribution in tubes. Dobson and Chato (1998) studied the condensation in smooth horizontal tubes. They pointed out that the heat transfer behavior depended significantly on the flow pattern. The gravity-dominated wavy flow prevailed at low mass fluxes, and film condensation was the dominant heat transfer mode. The bottom part of the tube that is immersed by liquid has less contribution to the heat transfer. At the highest mass fluxes, vapor shear dominated and annular or annular-mist flow prevailed over nearly the entire vapor quality range with forced-convective condensation as the prevailing heat transfer mode. This regime was characterized by heat transfer coefficients that decreased substantially with decreases in vapor qualities and mass fluxes. The heat transfer coefficients are quite sensitive to the liquid film thickness with the development of the condensation flow in the tube. At intermediate mass fluxes, wavy flow heat transfer behavior was observed at low qualities but became dominated by annular flow at higher mass fluxes. Recently, Lips and Meyer (2012) performed an experimental study of convective condensation of R134a in an 8.38 mm

* Corresponding author at: State Key Laboratory of Alternate Electrical Power System with Renewable Energy Sources, North China Electric Power University, Beijing 102206, China.
E-mail address: xjl@ncepu.edu.cn (J. Xu).

0301-9322/$ - see front matter © 2012 Elsevier Ltd. All rights reserved.
http://dx.doi.org/10.1016/j.ijmultiphaseflow.2012.04.003

inclined smooth tube. They presented flow patterns and heat transfer coefficients during condensation for different mass fluxes and vapor qualities for the whole range of inclination angles (from vertical downwards to vertical upwards). They found that the heat transfer coefficient is strongly affected by the liquid and vapor distributions and especially by the liquid thickness at the bottom of the tube for stratified flows. Thus it is necessary to develop a mechanistic model of flow pattern maps to achieve a predictive tool for the heat transfer coefficient in convective condensation in inclined tubes.

Qualitatively, for the gas–liquid or vapor–liquid two-phase flow in tubes, the liquid phase tends to populate near the wall and the gas phase tends to accumulate in the tube core. This conclusion can be verified by examining the void fraction distribution over the tube cross-section. Always, the void fractions attain the maximum value at the tube centerline and decrease with the distance away from the tube centerline. Such gas–liquid phase distribution is helpful to prevent the dryout at the wall surface for the boiling flow. However, for the condensation heat transfer in tubes, the large liquid thickness near the tube wall separates the tube wall from the saturated vapor, inducing a large thermal resistance due to the thick liquid thickness. In other words, the gas–liquid phase distribution does not harmonize with the condensation heat transfer. Various techniques to improve the condenser performance have been proposed in the literature and applied in many industry sectors. They can be found in consecutive review articles such as Cavallini et al. (2003), Dalkilic and Wongwises (2009), and Lips and Meyer (2011). The micro-groove tubes (Graham et al., 1999), micro-fin tubes (Cavallini et al., 2000), herringbone tubes (Miyara and Otsubo, 2002), helically corrugated tubes (Suriyan and Somchai, 2010) increase the heat transfer coefficient by mixing the fluid boundary layers and also by limiting the growth of fluid boundary layers close to the heat transfer surfaces. These techniques do not involve the flow pattern modulation in tubes.

Here we proposed a passive phase separation concept to create a distinct phase distribution in the tube cross section to yield good condenser performance. We suspended an empty mesh cylinder in a condenser tube, forming an inner region and an annular region between the tube wall and the mesh cylinder. The mesh cylinder acts as a gas bubble filter thus the gas phase flows in the annular region. Liquid can be sucked into the mesh cylinder through the miniature pores of the mesh by the capillary force. Thus the gas and liquid phases mainly populated near the tube wall region and the tube core region, respectively. Such phase distribution is thoroughly inverse to that in a conventional condenser tube. An adiabatic air–water two-phase flow experiment with horizontal orientation was performed to verify the phase distribution in tubes. It was found that when the liquid content is relatively large, the mesh cylinder can hold all the liquid with the tube wall surface fully contacted with the gas phase. If the liquid height is small, partial liquid can be sucked by the mesh cylinder, and the contact area between the tube wall and the gas is increased. The mesh cylinder can modulate the plug flow to form elongated saddle bubbles in the annular region. Besides, miniature bubbles can merge to form large bubbles in the annular region. For the later two cases, all the gas flow rate is flowing in the annular region and the inside mesh cylinder is the liquid. It is expected that such a condenser tube can significantly enhance the condensation heat transfer, which is being verified by the continuous condensation heat transfer experiment.

2. Design of the condenser tube and its working principle

In order to ensure the vapor phase having the largest possibility to contact with the tube inner wall, the central idea is to use a passive gas–liquid separator made of a single layer of mesh. Fig. 1 shows the design. Inside of the condenser tube mainly consists of an inner region and an annular region. Inlet of the mesh cylinder is a taper, or just a flat side mesh surface. Exit of the mesh cylinder is open to discharge the separated liquid. The inner region is empty. The mesh cylinder is uniformly suspended in the tube, but supporting structure may be needed.

When a gas (vapor)–liquid two phase flow stream is approaching the mesh cylinder region, the miniature pores have two functions. One is to prevent gas bubble entering the inner region, thus the gas phase is expected to flow in the annular region. The other is to suck the liquid towards the inner region. Due to the above two functions of the mesh pores, the gas and liquid phases are separated to flow in the two different regions. Such phase distribution is totally inverse to that in a conventional bare tube, and is very helpful for the condensation heat transfer because the saturated vapor can be directly contacted with the cold tube wall surface, forming the perfect thin film condensation heat transfer mode.

The mesh pore size should be small enough to prevent gas bubbles entering the inner region and pump the liquid towards the inner region. The effective pore diameter is suggested to have the criterion of $d_{eff} < \sqrt{\sigma/g(\rho_l - \rho_g)}$ (Xu and Zhang, 2005), where σ is the surface tension force, g is the gravity, and ρ_l and ρ_g are the liquid and gas densities, respectively. For most gas–liquid systems, d_{eff} is on the order of millimeter.

Fig. 2a shows the stainless steel mesh cylinder used for this experiment. The PPI (pores per inch) is 60. Each pore has a rectangular cross section with its size of 0.3 mm by 0.3 mm. The stainless steel ligament has a diameter of 0.1 mm. Fig. 2b is a picture of the fabricated mesh cylinder suspended in a glass tube. The inlet of the mesh cylinder is a flat pore surface. The outer diameter of the mesh cylinder is 9.32 mm.

3. Experiment

3.1. The test section

In order to study effect of the mesh cylinder on the phase distribution, two test sections are fabricated. Fig. 3a and b shows the test

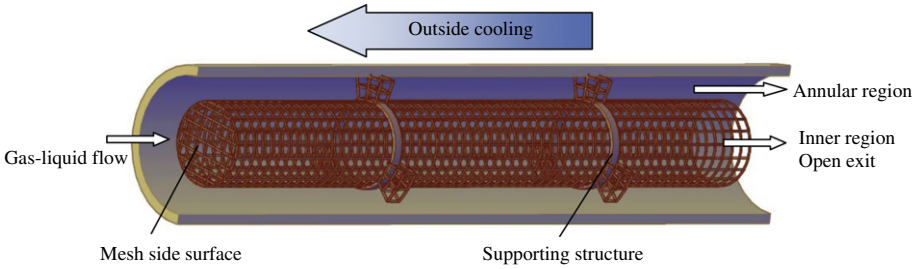

Fig. 1. The newly proposed condenser tube.

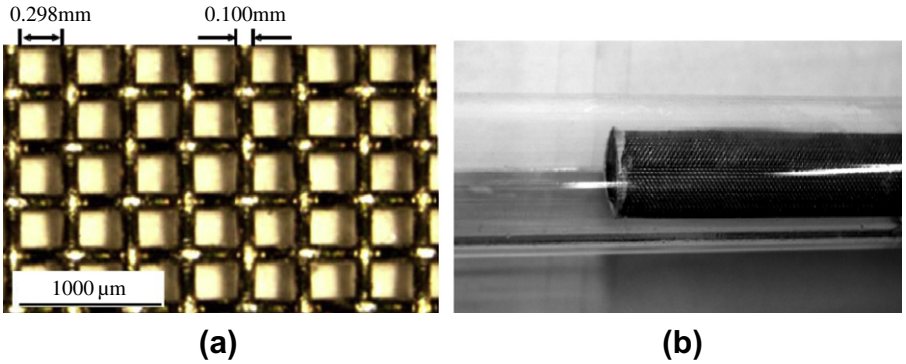

Fig. 2. Stainless steel mesh to fabricate the mesh cylinder ((a) for the mesh image measured by a microscope, (b) for the fabricated mesh cylinder inserted in a glass tube).

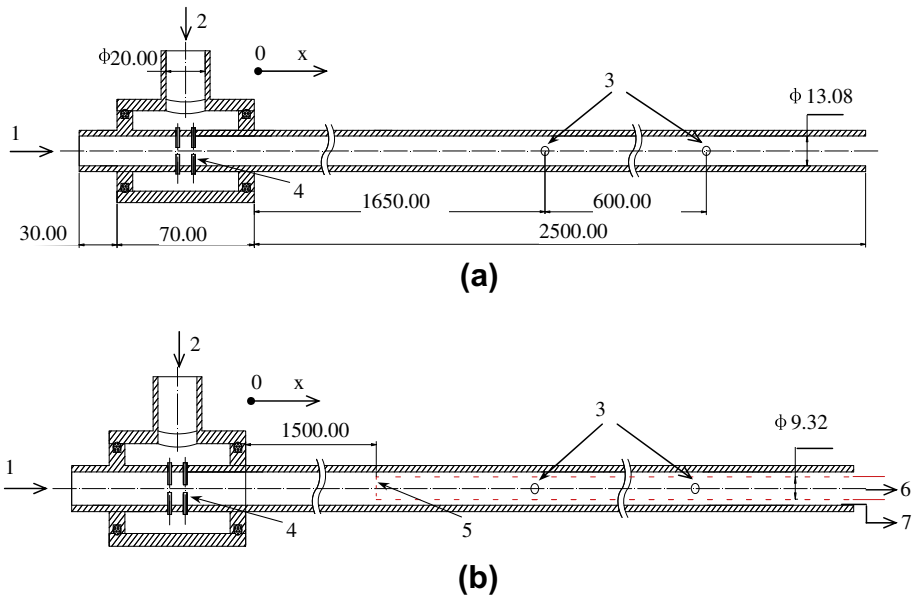

Fig. 3. Test sections for flow pattern measurement ((a) for the bare glass tube, (b) for the glass tube with a mesh cylinder inserted, 1: water inlet, 2: air inlet, 3: pressure tap, 4: needle, 5: mesh cylinder, 6: outlet fluid from the mesh cylinder to tank 1, 7: outlet fluid from the annular region to tank 2, note that all dimensions are in mm).

sections without and with the inserted mesh cylinder. Both test sections had a mixer at the entrance, having a short tube-in-tube geometry. Deionized water and air enter the test section from inlets 1 and 2, respectively. A set of miniature needles were uniformly distributed within the inner tube wall thickness (referred as 4 in Fig. 3). Air enters the annular region of the mixer and is discharged into the tube as air jets through the capillary holes of needles. A one-dimensional coordinate x was arranged with the original point starting from the mixer end. Two pressure ports (referred as 3 in Fig. 3) are arranged along the axial direction within a distance of 600 mm. The first pressure port starts from $x = 1650$ mm. A pressure drop transducer connects the two pressure ports to measure the pressure drop. The two test sections are made of glass so that the flow pattern visualization can be performed.

The glass tube had a total length of 2500 mm (not including the mixer), with an inner diameter of 13.08 mm and a tube wall thickness of 2.0 mm. For the second test section, the mesh cylinder is uniformly suspended in the glass tube by using three supporting structures (not shown in Fig. 3b). The mesh cylinder starts from $x = 1500$ mm, with an open end. The outer diameter of the mesh cylinder is 9.32 mm, forming an annular gap of 1.88 mm between the tube inner wall and the mesh cylinder. Two water tanks are used to collect the liquid flow rate from the inner region (referred as 6) and the annular region (referred as 7), respectively (see Fig. 3b).

3.2. The experimental setup

Fig. 4 shows the experimental setup. A water pump with variable speeds provides the water flow rate to the test section. A filter at the pump inlet prevents particles entering the test section. Depending on the flow rate for each run, the water flow rate was measured by one of the two turbine flowmeters, having the ranges of 0.2–2 m^3/h and 0.6–6 m^3/h respectively. An air compressor supplies the air flow rate to the test section. The air flow rate was measured by one of the three rotameters, with the ranges of 16–160 l/h, 0.1–1 m^3/h and 1–10 m^3/h respectively. The water and air flow rates enter the mixer of the test section. All the five flowmeters have accuracies of 0.5% within their own flow rate range. The pressure drop transducer has the accuracy of 0.1%. A high speed camera captures the flow patterns for the two test sections. A software (Photoshop CS5) analyzes the image pixels to locate the exact gas–liquid interface with a resolution of 1 μm.

The test section was exactly horizontally positioned. For the test section without the mesh cylinder inserted (see Fig. 4), the fluid at

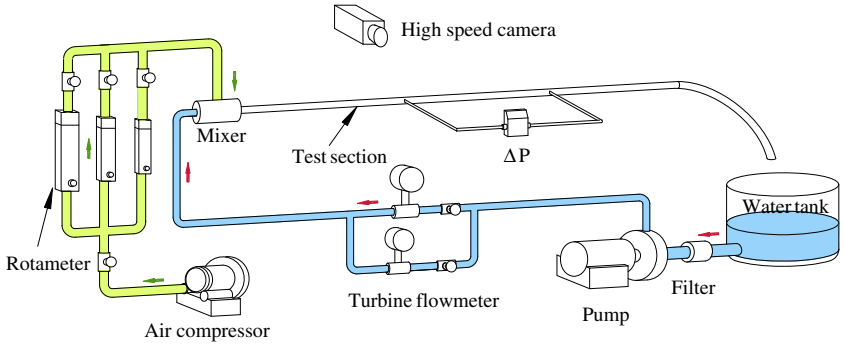

Fig. 4. Experimental setup for flow pattern measurement.

the test section outlet was collected by a tank. The outlet air was discharged into the environment directly but the water was collected by the tank. For the second test section, two tanks collect the water flow rates from both the inner region and annular region respectively, which was described in Section 3.1 but not shown in Fig. 4.

The superficial velocities of liquid and gas phases are defined as

$$J_l = \frac{Q_l}{A}, \quad J_g = \frac{Q_g}{A} \tag{1}$$

where Q_l and Q_g are the volume flow rates of liquid and gas phases, A is the tube cross section area. During this experiment, J_l and J_g have the ranges of 0.01–2.0 m/s and 0.1–10 m/s respectively.

4. Results and discussion

4.1. Flow patterns in the horizontal glass tube

Many text books on the two-phase flow and heat transfer describe the flow patterns in horizontal tubes. Fig. 5 shows typical flow patterns in the present horizontal tube. Over the ranges of flow rates for gas and liquid phases, stratified smooth, stratified wavy, plug, slug and annular flows are observed. These flow patterns are described as follows:

(a) *Stratified smooth flow*. This pattern only occurs at very low liquid and gas velocities. The two phases flow separately with a relatively smooth interface.

(b) *Stratified wavy flow*. As the gas velocity is increased the interface becomes disturbed by waves traveling in the flow direction.

(c) *Plug flow*. Plugs of gas, formed from many bubbles coalescing, flow in continuous liquid phase.

(d) *Slug flow*. A further increase in gas velocity causes the waves at the interface to be picked up to form a frothy slug which is populated along the channel at a high velocity. The upper surface of the tube behind the wave is wetted by a residual film which drains into the bulk of the liquid. A set of bubble slugs are separated by specific length of liquid bridges.

(e) *Annular flow*. A still higher gas velocity results in the formation of a gas core with a liquid film around the periphery of the pipe. The film may or may not be continuous around the entire circumference but it will, of course, be thicker at the base of the pipe. Miniature liquid droplets may be entrained in the gas core.

Fig. 6 shows the flow pattern map in the 13.08 mm diameter tube. Besides, the transition boundaries of various flow patterns are marked according to Mandhane et al. (1974). The present measured flow patterns generally match the transition boundaries reported by Mandhane et al. (1974).

4.2. Flow pattern modulation by the inserted mesh cylinder

4.2.1. Stratified flow pattern modulation

4.2.1.1. The full liquid capture case. It is observed that there are two modes of stratified flow pattern modulations by the mesh cylinder.

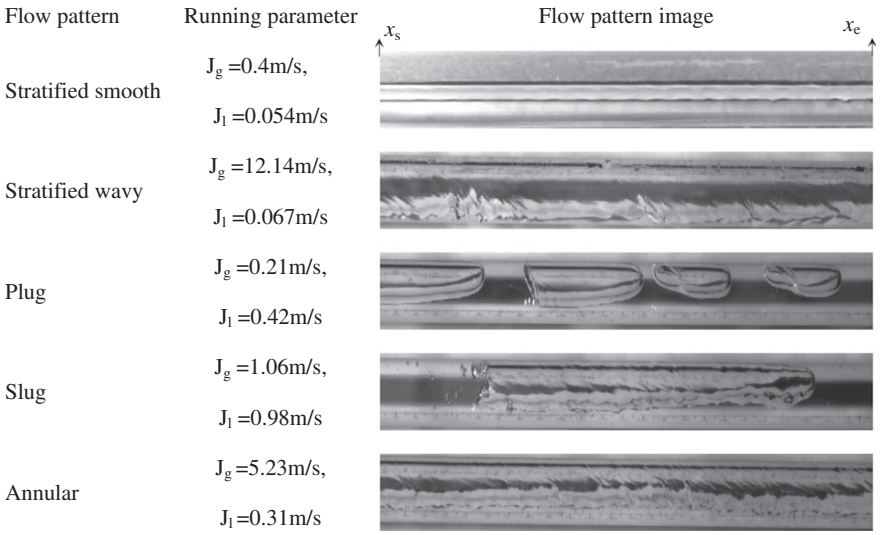

Fig. 5. Flow pattern observed in the bare horizontal glass tube (x_s = 1950 mm, x_e = 2190 mm, x_s and x_e refer the start and end locations of the illustrated image, respectively).

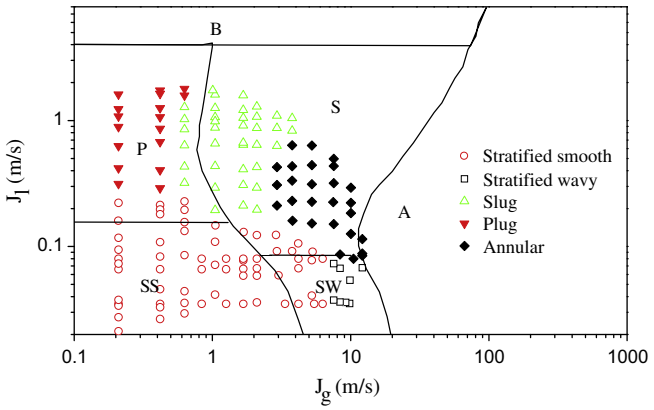

Fig. 6. The flow pattern map in the bare horizontal glass tube and comparison with Mandhane et al. (1974, B: Bubbly flow region, P: Plug flow region, S: Slug flow region, A: Annular flow region, SS: Stratified smooth flow region, SW: Stratified wavy flow region).

One is the full liquid capture mode (called the "gas-floating-liquid" mode). The other is the partial liquid capture mode. Fig. 7 shows a set of images for the stratified flow pattern modulation in the millisecond timescale for the first mode. By carefully examining pixels of the visualized images, we could identify the liquid height from the tube bottom along the flow direction. The visualization zone starts from x_s = 1455 mm and ends at x_e = 1555 mm with an axial distance of 100 mm. It is noted that the O-ring supporting structure is located at x = 1560 mm, that is beyond of the visualization zone of Fig. 7. Three cross sections are illustrated with marked liquid and gas phase distribution. The liquid height was 5.88 mm for the stratified flow at the mesh cylinder upstream (see the A–A cross section in Fig. 7). Once the stratified flow reaches the mesh cylinder surface, the capillary pumping effect causes different liquid levels in the inner region and the annular region of the tube (see the B–B cross section in Fig. 7). For instance, the liquid height was 6.48 mm in the inner region but it was only 3.45 mm in the annular region over the B–B cross section. The liquid suction process is over within an axial distance of 13 mm, followed by the steady state flow. The C–C cross section demonstrates the state under which all the liquid is within the mesh cylinder, floated by the gas phase in the annular region, referred as the "gas-floating-liquid" mode. The capillary force created by mesh pores is balanced by the liquid gravity force in the vertical direction. We note that the contact area between tube inner wall and gas is 218.4 cm^2/m in the upstream A–A cross section, but it is increased to 433.3 cm^2/m in the downstream C–C cross section. It is also noted that the contact area between the gas and liquid interface per unit flow length is 174 cm^2/m in the downstream C–C cross section, which is larger than the value of 130 cm^2/m in the upstream A–A cross section without inserting the mesh cylinder (see Fig. 7), causing the increased momentum exchange between the gas and liquid phases. In other words, the shear force acting on the liquid phase is increased when the mesh cylinder is involved, causing the faster liquid transport in the downstream mesh cylinder region.

In order to further verify the "gas-floating-liquid" mode, we collect the fluids at both outlets of the mesh cylinder (inner region) and annular region of the tube respectively. It is found that the liquid flow rate from the mesh cylinder outlet is exactly equal to that measured by the liquid flowmeter at the pump outlet. Besides, it is found that there is no any liquid coming out from the annular region of the tube (see Fig. 8). The "gas-floating-liquid" mode is very helpful for the condensation heat transfer. This is because the entire tube inner wall surface is thoroughly covered by the vapor phase, ensuring the perfect thin liquid film condensation heat transfer between the cold wall surface and the vapor.

4.2.1.2. The partial liquid capture case. It is observed that the "gas-floating-liquid" mode takes place at relatively higher liquid level in the horizontal tube. Generally, the liquid height is decreased with decreases in the liquid superficial velocities. At relatively lower liquid height, part of liquid can be captured by the mesh

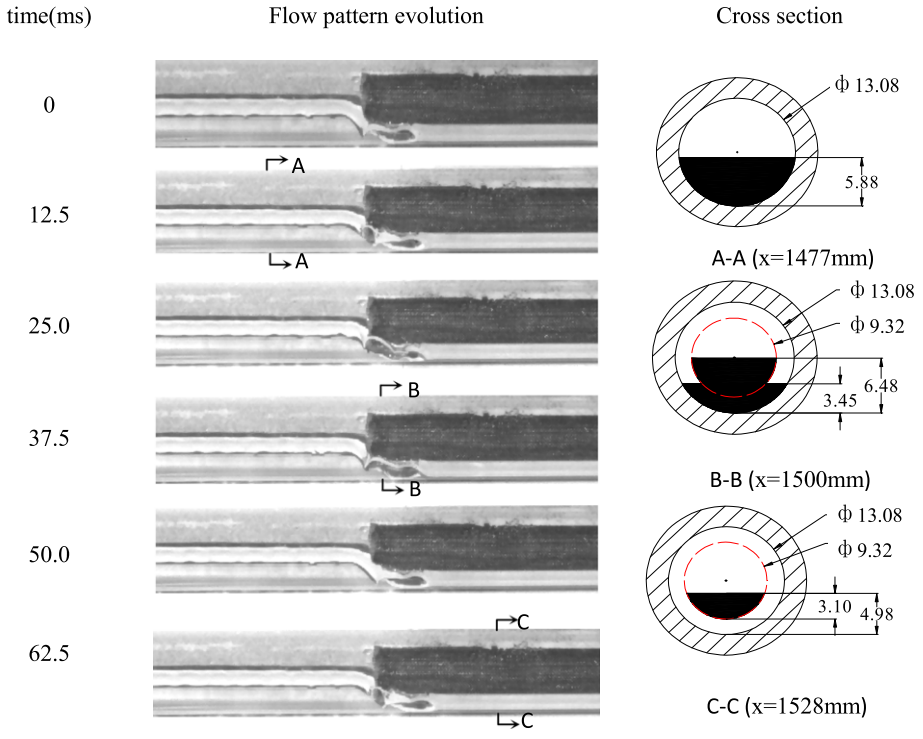

Fig. 7. Flow pattern evolution in different cross sections (full liquid capture case, J_g = 0.335 m/s, J_l = 0.054 m/s, x_s = 1455 mm, x_e = 1555 mm).

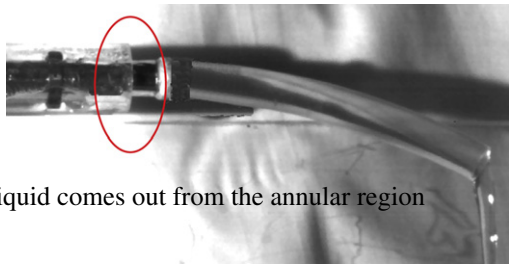

Fig. 8. Image for outlet fluid from the mesh cylinder and annular region of the tube.

cylinder. An initial liquid height was 4.22 mm in the bare tube section at the gas and liquid superficial velocities of 0.335 m/s and 0.035 m/s respectively (see the A–A cross section in Fig. 9). Once the stratified flow encounters the mesh cylinder, the capillary pumping effect causes a higher liquid height of 5.56 mm in the mesh cylinder but a lower liquid height of 1.88 mm in the annular region (see the B–B cross section in Fig. 9). Further evolution of the phase distribution of the gas and liquid yields the liquid heights of 5.56 mm in the mesh cylinder and 2.45 mm in the annular region (see the C–C cross section in Fig. 9). At the steady state the inner region and annular region share the same liquid height of 3.20 mm (see the D–D cross section in Fig. 9). By comparing Figs. 7 and 9, it is seen that the initial liquid wetting perimeter along the mesh cylinder circumference plays an important role on the liquid hold up in the gravity direction (vertical direction). A lower liquid superficial velocity may not cause the full "gas-floating-liquid" mode. Even though the liquid is not fully "floated" by gas, the contacted area between the tube inner wall surface and the gas phase is increased with the help of the mesh cylinder by comparing the A–A and B–B cross sections (see Fig. 9).

It is seen that the O-ring supporting structure has local effect on the gas–liquid phase distribution (see Fig. 9). Because there is a miniature gap between the supporting structure and the mesh cylinder, the liquid height in the annular region is slightly increased near the supporting structure area. However, the present study found that when the flow approaches the steady state, the liquid heights inside and outside of the mesh cylinder are the same, no matter where is the supporting structure and if there is a supporting structure.

The liquid separation ratio k is defined as the mass flow rate of liquid at the mesh cylinder outlet divided by the total mass flow rate of liquid. Fig. 10 illustrates that the liquid separation ratios are dependent on both the superficial velocities of liquid and gas phases. The full liquid capture mode, i.e. the "gas-floating-liquid" mode appears at higher liquid superficial velocity of 0.054 m/s over the gas superficial velocities from 0.1 to 1.0 m/s. For the partial liquid capture mode, the liquid separation ratios are increased with increases in both the superficial velocities of liquid and gas phases. At the gas superficial velocity of 1.0 m/s, k attains 0.5–0.8.

4.2.2. Intermittent flow pattern modulation

Intermittent flow pattern refers the plug flow and slug slow. The two flow patterns share some common features. But plugs are shorter and populate in the upper part of the horizontal tube. Slugs are longer and occupy the whole cross section of the horizontal tube. For both flow patterns, consecutive plugs or slugs are separated by liquid bridges. For the convective condensation heat transfer with plug flow or slug flow in horizontal tubes, the condensation heat transfer coefficient is lower when liquid bridges are sweeping the inner wall surface. Besides, because plugs may not envelop the whole circumference of the tube inner wall surface, heat transfer coefficients during the plug traveling process is not too high.

We study the phase distribution modulation in plug and slug flow regimes. A typical case was shown in Fig. 11 for J_g = 0.21 m/s and J_l = 0.44 m/s. Flow pattern images are given at the upstream, entrance and downstream of the mesh cylinder. We track the first plug bubble with its length of 60 mm. The liquid bridge following the plug bubble is 55 mm (see Fig. 11a). When the plug bubble is

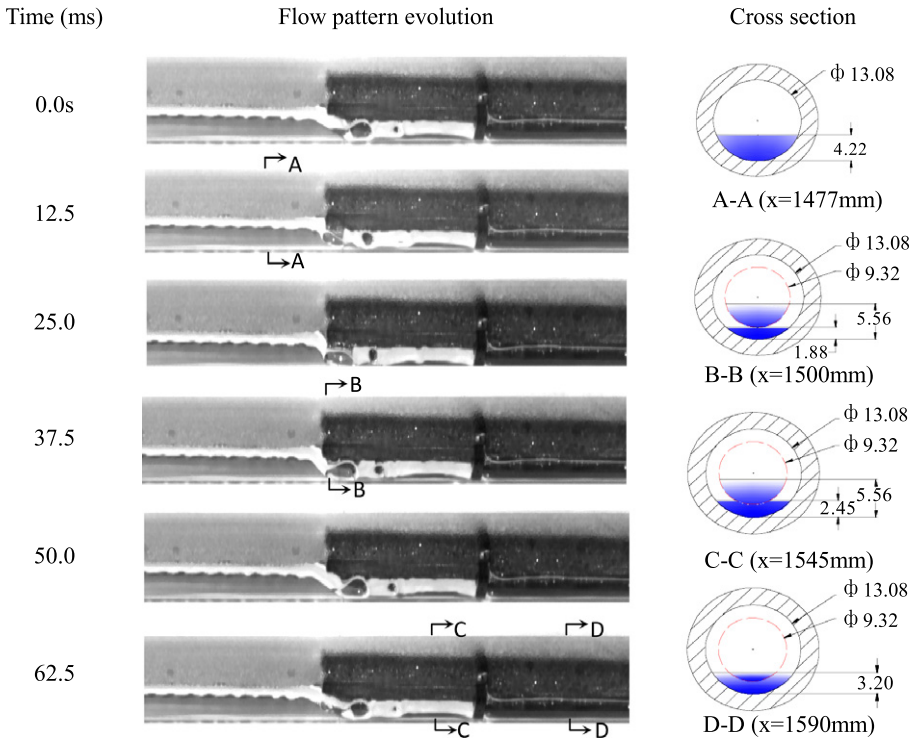

Fig. 9. Flow pattern evolution in different cross sections (partial liquid capture case, J_g = 0.335 m/s, J_l = 0.035 m/s, x_s = 1435 mm, x_e = 1615 mm).

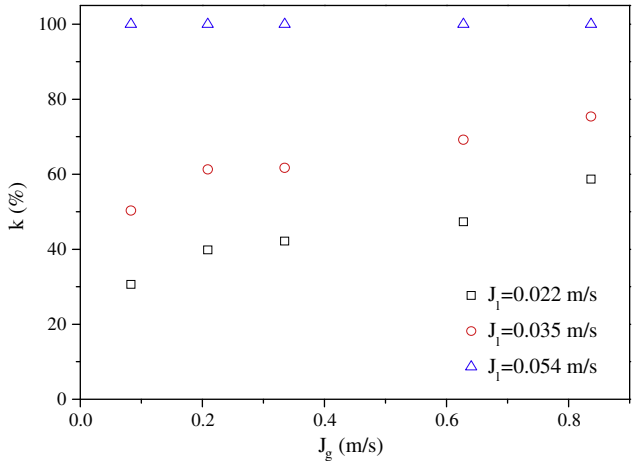

Fig. 10. The liquid separation ratios versus superficial velocities of liquid and gas.

crossing the mesh cylinder surface, it is modulated to have three parts: a saddle bubble front in the annular region, a bubble neck at the annular region entrance, and a plug bubble tail out of the mesh cylinder area (see Fig. 11b). Fig. 11c illustrates the full confinement of the saddle bubble in the annular region. The elongated saddle bubble has a length of 105 mm, which is 1.75 times of that shown in bare tube by comparing Fig. 11a and c. The liquid bridge length is less changed to have a length of 55 mm.

Fig. 12 identifies the saddle bubble formation process. State A is the time before a plug bubble encounters the mesh cylinder surface. States B and C show that the plug bubble is crossing the mesh cylinder entrance, in which the bubble neck is formed in state C. A full saddle bubble is formed in state D. Over the data range in plug and slug flow patterns, the gas phase never enters the inner region of the mesh cylinder. Fig. 13 shows that outlet of the inner region is the liquid without any gas bubble. All gas flow rate is flowing in the annular gap between the tube inner wall and the mesh cylinder. The liquid separation ratio can be high up to 90% at small liquid superficial velocity of 0.1 m/s (see Fig. 14). It is decreased and attains a constant value of 0.55 with increases in the liquid superficial velocities. Generally the liquid separation ratio is mainly dependent on the liquid superficial velocities, weakly dependent on the gas superficial velocities. This means that both inertial force and surface tension force influence the liquid suction process towards the mesh cylinder. The Weber number represents the inertial force relative to the surface tension force, which is defined as

$$We_l = \frac{\rho_l J_l^2 d_{eff}}{\sigma}, \quad We_g = \frac{\rho_g J_g^2 d_{eff}}{\sigma} \tag{2}$$

Considering the liquid superficial velocities of J_l in the range of 0.1 to 1.0 m/s for the plug flow pattern modulation, the Weber number based on J_l is in the range of 0.4–40, indicating that both inertial force caused by liquid phase and surface tension force have influence on the liquid suction process. For lower liquid superficial velocities, the liquid separation ratio is higher due to the stronger effect of surface tension force. The liquid separation ratios are decreased and attain a constant value of about 0.55 with increases in the liquid superficial velocities due to the enhanced influence of the inertia force by the liquid phase. On the other hand, the Weber number based on the gas superficial velocity is in the range from 4×10^{-5} to 4×10^{-3} with J_g in the range from 0.1 to 1.0 m/s, indicating that the surface tension force is much stronger to influence the liquid suction process compared with the inertia force by the gas phase. Thus the liquid separation ratios are weakly dependent on the gas superficial velocities.

We note that the liquid separation ratios have different trends versus superficial velocities of gas and liquid phases for the modulations of intermittent flow pattern and stratified flow pattern. For the later case, the liquid separation ratios are increased with increases in both the superficial velocities of gas and liquid phases.

For the condensation in a horizontal bubble with an inserted mesh cylinder, the condensation heat transfer can be significantly enhanced by the following two mechanisms: (1) the significantly increased contact area between the tube inner wall and the vapor phase, (2) the increased moving speed of the saddle bubble in the annular region.

4.2.3. Bubbly flow pattern modulation

Bubbly flow occurs at the end of a condenser tube and is an important flow pattern to influence the condenser performance. Miniature bubbles are difficult to be fully condensed, requiring a longer condenser tube length. Considering an Organic Rankine Cycle system, if miniature bubbles are not fully condensed, they will attack the rotating blades of the fluid pump, shortening the pump lifetime.

The thermal nonequilibrium between liquid and vapor phases exist during the bubble condensation process. Usually miniature

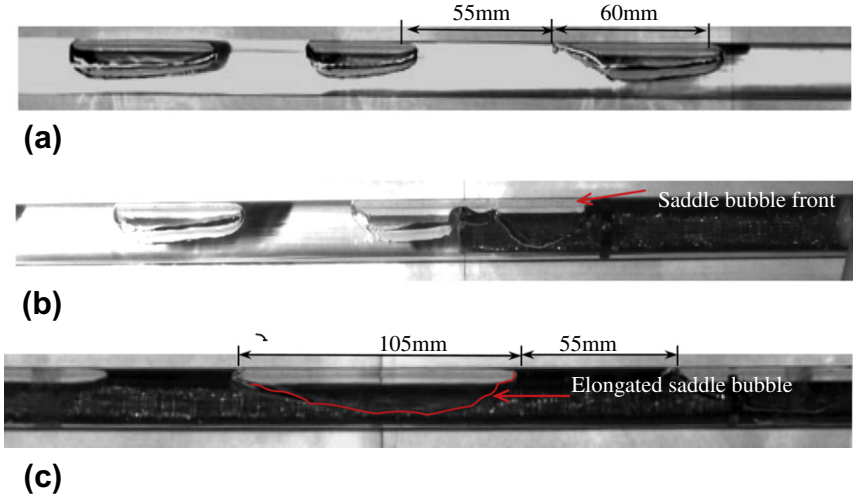

Fig. 11. Flow pattern modulation by the mesh cylinder with J_g = 0.21 m/s, J_l = 0.44 m/s ((a) flow pattern at the mesh cylinder upstream with x_s = 960 mm and x_e = 1275 mm, (b) flow pattern at the mesh cylinder entrance with x_s = 1340 mm and x_e = 1656 mm, (c) flow pattern in the mesh cylinder downstream with x_s = 1915 mm and x_e = 2220 mm).

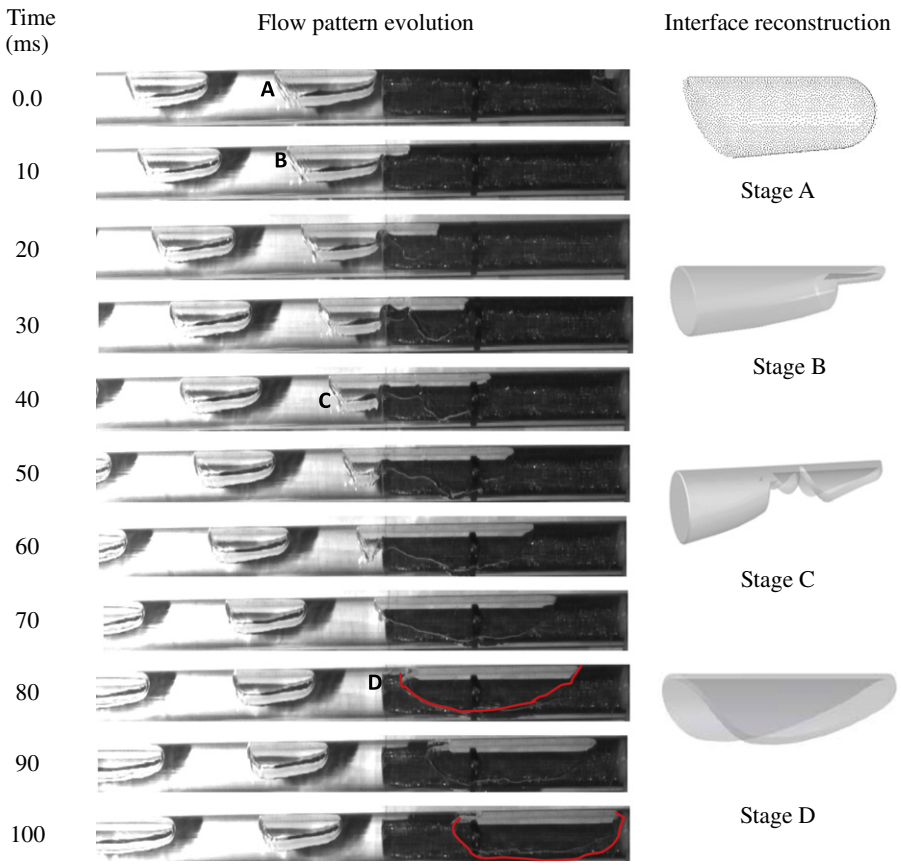

Fig. 12. The flow pattern evolution modulated by the mesh cylinder (J_g = 0.21 m/s, J_l = 0.44 m/s, x_s = 1335 mm, x_e = 1655 mm).

Fig. 13. Image at the mesh cylinder outlet and annular region for intermittent flow pattern.

bubbles are suspended in the continuous liquid phase. The decrease of the bubble size is strongly dependent on the temperature difference between the two phases. Bubble condensation in subcooled liquid is controlled either by inertia or by heat diffusion. In a highly subcooled liquid at the cost of large heat transfer area, bubbles rapidly collapse satisfying the Rayleigh solution. If the subcooling is low, bubble collapse takes longer and the process is governed by diffusion of the latent heat away from the interface. As noted by Vasil'ev (2003) and Kalman and Mori (2002), the ratio of the Peclet to Jakob number (Pe/Ja) determines the heat transfer mechanism where $Pe/Ja \gg 1$ leads to the heat diffusion mechanism. But inertia dominates if $Pe/Ja < 1$. Both mechanisms are important if $Pe/Ja \sim 1$.

The mesh cylinder modulates isolated miniature bubbles to form larger merged bubbles that are directly contacted with the cold tube inner wall surface. Thus the perfect thin film condensation heat transfer mode is ensured between the tube wall and the vapor, similar to the annular flow pattern to hold high heat transfer coefficient. Fig. 15 shows isolated miniature bubbles at

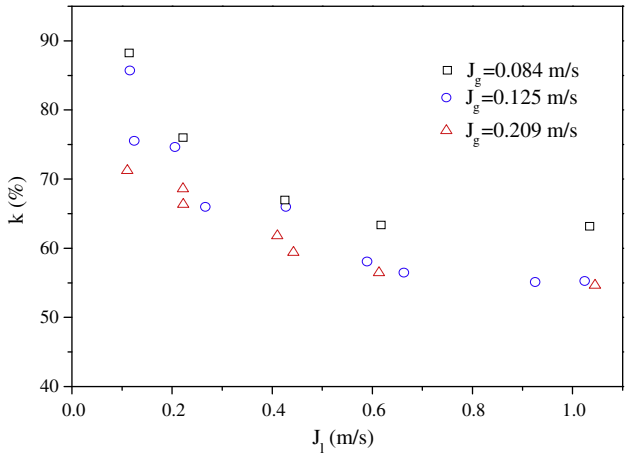

Fig. 14. The liquid separation ratio for intermittent flow pattern.

the mesh cylinder upstream. They begin to be close with each other when they approach the mesh cylinder, and are fully merged in the annular region of the tube. Fig. 16 shows the liquid phase without any gas bubbles at the mesh cylinder outlet. It is found that for the bubble flow pattern in the present data ranges of superficial velocities of liquid and gas phases, the liquid separation ratios are almost constant to have the value of 0.55.

4.2.4. Explanation of the phase separation concept by the mesh cylinder

There are two mechanisms for the mass and momentum transfer across the mesh pore surface. If the single-phase flow (either

gas or liquid) is continuously approaching the mesh pore surface, the mass and momentum transfer across the two sides of the mesh pores obeys the principle of the single-phase fluid dynamics. Under such circumstance, nothing prevents gas or liquid flowing across the mesh pores. The mass flow rate is dependent on the static pressure difference and flow field across the two sides of mesh pores.

However, when an intermittent flow (plug, slug or bubble) interacts with the mesh pores, the bubbles are difficult to enter the mesh pores if the mesh pore surface is wet. This is based on the fact that the surface energy of the gas bubble is increased when it is forced to move from a relative large space into a small space when a curved gas–liquid interface is within the mesh pores. Here we gave an explanation on the prevention of bubbles entering the mesh pores and the liquid suction through the mesh pores for an initially wet mesh pore surface and intermittent flows. The stratified flow pattern modulation by the mesh cylinder is easy to explain. The increased liquid height within the mesh cylinder is caused by the capillary pumping effect in the vertical direction which is perpendicular to the flow direction, similar to that a higher liquid height in a capillary tube can be sustained when the capillary tube is standing in a liquid pool.

4.2.4.1. The bubble is prohibited to enter the mesh cylinder for intermittent flows. Considering a large bubble with its diameter identical to the condenser tube is penetrating a rectangular mesh pore (see Fig. 17a), the surface energy of the gas bubble between state A and B is expressed as

$$dE = \sigma 4wds2 - \sigma\pi Dds1 \tag{3}$$

where E is the surface energy, D is the tube inner diameter (D = 13.08 mm), w is the width of the rectangular mesh pore (w = 0.3 mm). The mass conservation yields the following equation by neglecting the gas bubble density variation:

$$w^2 ds2 = \frac{\pi D^2}{4} ds1 \tag{4}$$

On the other hand, the work required to transform the gas bubble from state A to state B is

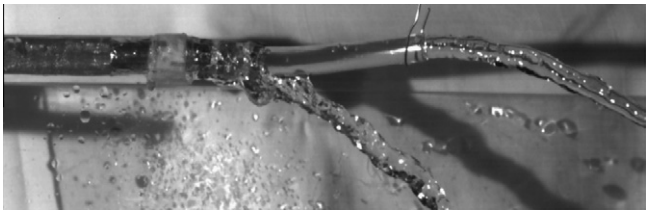

Fig. 16. Outlet fluid flow at the outlets of the mesh cylinder and annular region (J_g = 0.067 m/s, J_l = 0.9 m/s).

$$dK = P_1 \frac{\pi D^2}{4} ds1 - P_2 w^2 ds2 \tag{5}$$

The dK being equal to dE yields the pressure difference as

$$P_1 - P_2 = 4\sigma\left(\frac{1}{w} - \frac{1}{D}\right) \tag{6}$$

It is seen from Eq. (6) that because $D \gg w$, the second term of the right side of Eq. (6) contributes much less to the pressure difference. Giving σ = 0.07275 N/m for air–water system at 20 °C and w = 0.3 mm, $P_1 - P_2$ = 970 Pa. This indicates that the pressure difference of more than 970 Pa is needed to penetrate the front bubble interface in mesh pores.

Similarly, if a bubble in the annular region of the condenser tube is penetrating a mesh pore, the pressure difference can also be deduced as (Tsai and Lin, 2002)

$$P_1 - P_2 = 4\sigma\left(\frac{1}{w} - \frac{1}{\delta}\right) \tag{7}$$

where δ is the gap distance of the annular region (δ = 1.88 mm here). Because δ is about six times of w, $P_1 - P_2$ is also on the order of 1 kPa.

Eqs. (6), and (7) indicate that a large pressure drop of about 1 kPa should be needed to penetrate a bubble front in the mesh pore. It is noted that the penetrating of a bubble front over the mesh pore does not mean that such a bubble can successfully enter the mesh cylinder. There are two possible mechanisms for the penetrating bubble to be separated from its mother bubble outside of

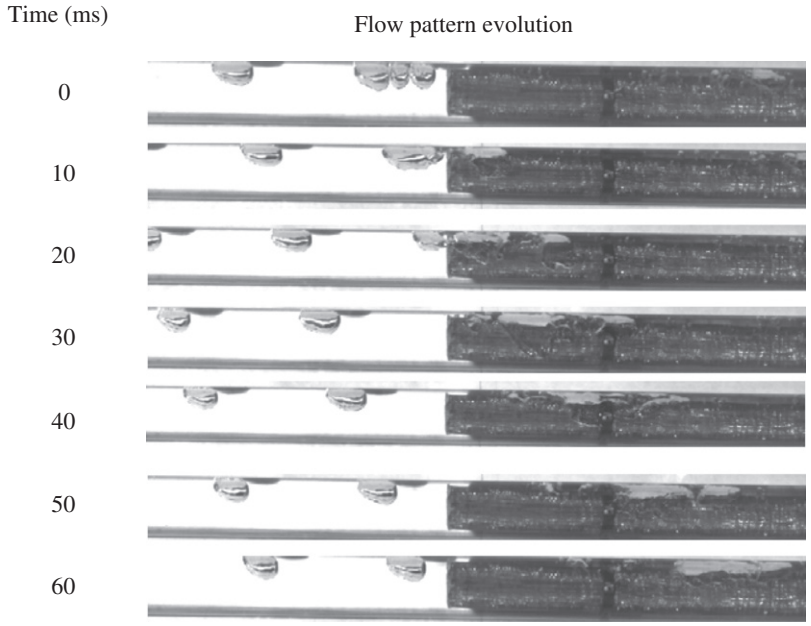

Fig. 15. Bubble coalescence process in the bubbly flow region (J_g = 0.067 m/s, J_l = 0.9 m/s, x_s = 1390 mm, x_e = 1630 mm).

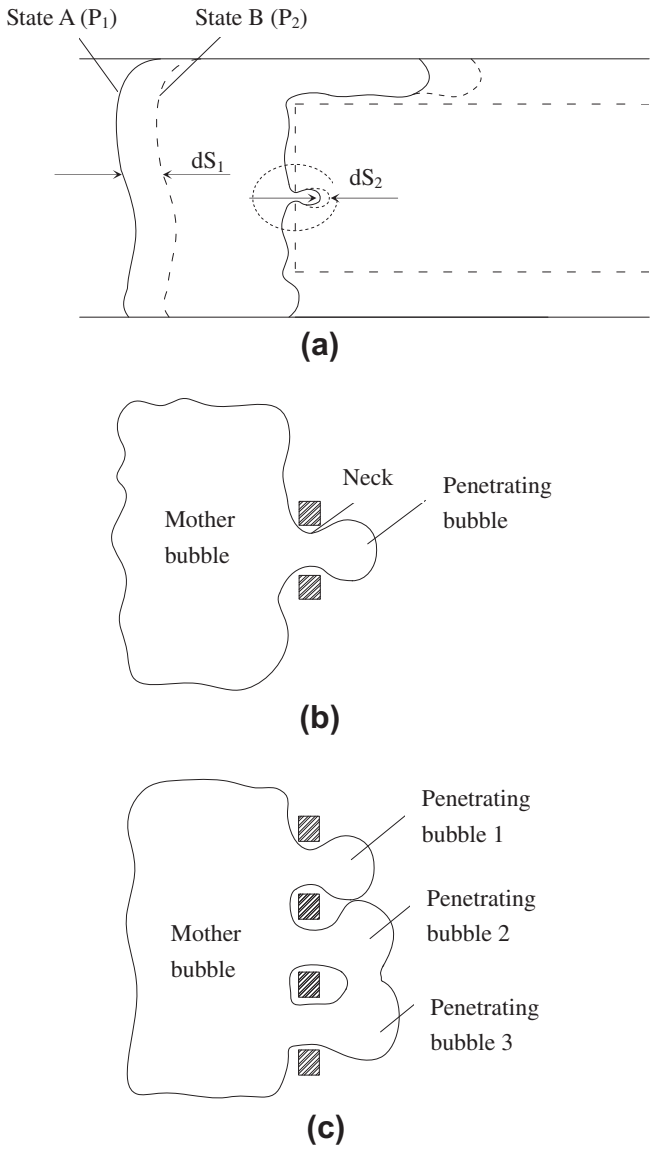

Fig. 17. The mechanism of the mesh pores preventing bubbles entering the mesh cylinder ((a) for pressure difference analysis for a bubble front penetrating over the mesh pore, (b) for the mechanism for the breakup of the bubble neck, (c) for the coalescence mechanism of many bubble fronts to form large bubble).

the mesh cylinder: (1) the viscous force from surrounding liquid (see Fig. 17b), (2) the coalescence of many bubble fronts from the mesh pore array to form a larger bubble (see Fig. 17c).

The capillary number (Ca) demonstrates the viscous force of the continuous phase (liquid here) relative to the surface tension force, which is expressed as $Ca = u_l\mu_l/\rho_l\sigma$, where u_l is the liquid velocity acting on the gas bubble, μ_l is the liquid viscosity. Having $\mu_l = 1.01 \times 10^{-3}$ Pa·s, $\rho_l = 1000$ kg/m^3 for water, and $\sigma = 0.07275$ N/m at the air–water interface, the Ca number is in the range of 1.4×10^{-6}–1.4×10^{-5} with the liquid velocities in the range of 0.1–1.0 m/s. The Ca number is so small that the bubble neck cannot breakthrough the mesh pore (see Fig. 17b).

Alternatively, the coalescence of many bubble fronts can form a large bubble, which can be separated from its mother bubble and enter the mesh cylinder (see Fig. 17c). The second mechanism should be verified by the future experiment. The prohibition of the bubble coalescence is to ensure that the bubble fronts should be within the mesh pores so that the bubble fronts never contact with each other.

4.2.4.2. Liquid suction through mesh pores. The proposed condenser tube involves the liquid suction process towards the mesh pores. We consider a large bubble with its front traveling ahead in the annular region (see Fig. 18a). The mesh pores are numbered as the index $i = 1,2,3\ldots I$ along the flow direction. The bubble front is consecutively sweeping the mesh pores. For instance, the bubble front does not reach the #5 mesh pore at $t = t_0$ (see Fig. 18a), with the bubble interface indicated by the black color. The A–A cross section is full of liquid before the bubble front reaches the #5 mesh pore (see Fig. 18b). A curved gas–liquid interface is formed within the #5 mesh pore at $t_1 = t_0 + \Delta t$, where $\Delta t = w/u_g$, w is the mesh pore width and u_g is the moving speed of the bubble front. The bubble interface is indicated by the red curve. Fig. 18c shows the phase distribution at $t = t_1$, indicating a thin liquid film on the tube wall and a liquid core with curved gas–liquid interface. There are N mesh pores along the circumference direction in the A–A cross section.

There is no liquid sucked into the mesh cylinder when the static gas–liquid interface is within the mesh pores (#1, 2, 3 and 4 mesh pores in Fig. 18a). But liquid can be captured by mesh pores during the dynamic sweeping process of the bubble front from the time without an interface at $t = t_0$ to the time with an interface at $t = t_1$. Following $t > t_1$ no liquid can be sucked into the #5 mesh pore but liquid can be sucked into the next mesh pore.

The capillary pressure is changed during the dynamic interface formation process when the bubble front is sweeping the mesh pore. The detailed analysis shall be performed using the interface tracking technique such as VOF method. Here we use the porous media theory to estimate the liquid suction velocity and flow rate during such interface variation process. The capillary pressure is zero at $t = t_0$ (see Fig. 18b) and it has the following expression at $t = t_1$ (see Fig. 18c):

$$\Delta p_c = 4\sigma \cos\alpha / d_{eff} \tag{8}$$

Eq. (8) is cited from Larson and Morrow (1981). Δp_c is the capillary pressure, d_{eff} is the effective pore diameter of the mesh, and α is the wetting angle.

The contact angle for stainless steel mesh pore surface and water was measured to be 81°, which is different from the value of 70° for stainless steel plate and water (see Fig. 19). It is noted that Fig. 19b shows a water droplet on a dry mesh pore surface. The liquid droplet will be quickly spreading over the mesh pore surface if such a droplet is impinging an initially wet mesh pore surface and the contact angle approaches zero under such circumstance.

Based on the Darcy's equation, the pressure drop for the liquid flow through mesh pores is

$$\Delta p_l = \frac{\mu_l u_{l,s}}{K}\Delta x \tag{9}$$

where $u_{l,s}$ is the liquid suction velocity through mesh pores, Δx is the mesh wire thickness, K is the porous permeability, which is expressed as

$$K = \frac{\varepsilon d_p^2}{32} \tag{10}$$

where ε is the porosity of a single layer mesh, d_p is the pore diameter. The balance of the capillary pressure and pressure drop for liquid suction through mesh pores, i.e. $\Delta p_c = \Delta p_l$, yields the following expression for the liquid suction velocity:

$$u_{l,s} = \frac{\varepsilon\sigma d_p^2 \cos\alpha}{8\mu_l \Delta x d_{eff}} \tag{11}$$

Therefore the mass flow rate of the liquid suction through mesh pores are estimated as

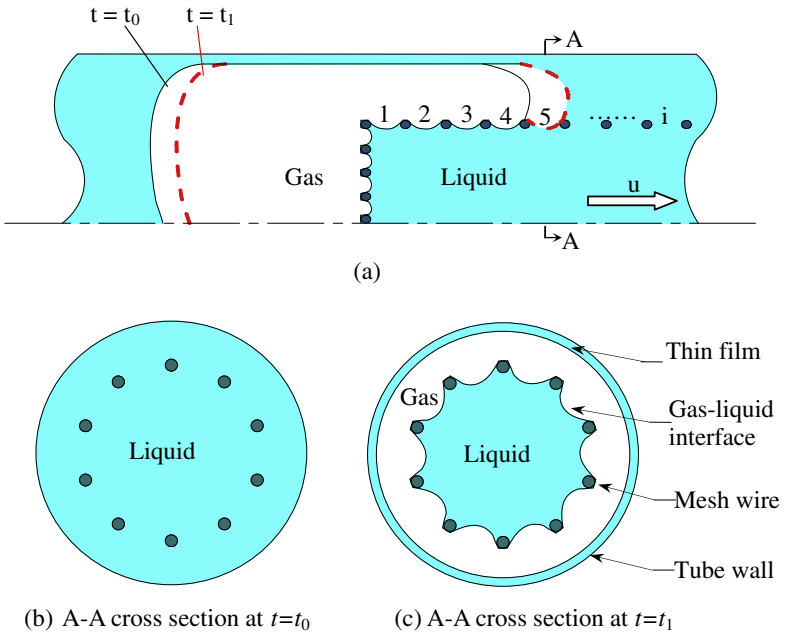

Fig. 18. The liquid suction caused by dynamic process of bubble front sweeping the mesh pores.

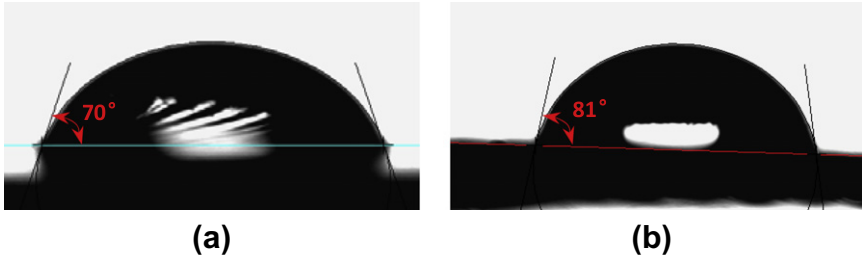

Fig. 19. Contact angles for a water droplet on the plain stainless steel plate (a) and mesh pore surface (b).

$$m = \rho_l u_{l,s} N A_c = \frac{N \rho_l \varepsilon w^2 d_p^2 \sigma \cos\alpha}{8 \mu_l d_{eff} \Delta x} \tag{12}$$

where N is the number of mesh pores along the circumference direction in the A–A cross section, A_c is the cross section area of a single mesh pore, which equals to w^2. Considering the present application for $\alpha = 81°$, the suction mass flow rate of the liquid is roughly estimated to 10.8 g/s for a single bubble front sweeping the mesh pores in the annular region. It is noted that there are many elongated bubbles flowing in the annular region.

5. Conclusions

We proposed a passive phase separation concept to modulate the flow pattern in a condenser tube. An empty mesh cylinder is suspended in the condenser tube, dividing the tube cross section into an inner region and an annular region. Gas bubble can be prevented to enter the mesh cylinder but liquid can be sucked towards the mesh cylinder through the mesh pores. An air–water two-phase flow experiment was performed to verify the idea. If there is a relatively higher liquid level in the bare horizontal tube, all liquid can be captured by the mesh cylinder to form the "gas-floating-liquid" mode. For a lower liquid height in the horizontal tube, partial liquid can be sucked by the mesh cylinder, and the contact area between the tube wall and the gas is increased. Elongated saddle bubbles are formed in the annular region to envelop the mesh cylinder when plug bubbles interact with the mesh cylinder surface. Miniature bubbles can merge to form large bubbles in the annular region for the isolated bubbly flow pattern modulation. The gas phase only flows in the annular region for the later two cases. For all the above flow pattern modulations by the mesh cylinder, the condensation heat transfer should be enhanced due to the gas phase populated near the tube inner wall surface, thus the perfect thin film condensation heat transfer mechanism can be ensured.

Acknowledgements

This work was supported by the National Basic Research Program of China with the contract number of 2011CB710703, the natural science foundation of China with the contract number of 51106050, and the natural science foundation of China with the contract number of 51006035.

References

Cavallini, A., Del Col, D., Doretti, L., 2000. Heat transfer and pressure drop during condensation of refrigerants inside horizontal enhanced. Int. J. Refrig. 23, 4–25.
Cavallini, A., Censi, G., Del Col, D., Doretti, L., Longo, G.A., Rossetto, L., Zilio, C., 2003. Condensation inside and outside smooth and enhanced tubes-a review of recent research. Int. J. Refrig. 26, 373–392.
Dalkilic, A.S., Wongwises, S., 2009. Intensive literature review of condensation inside smooth and enhanced tubes. Int. J. Heat Mass Transfer 52, 3409–3426.
David, J.S., Neil, L., 2010. Organic rankine cycle working fluid considerations for waste heat to power applications. ASHRAE Trans. 116, 525–533.

Dobson, M.K., Chato, J.C., 1998. Condensation in smooth horizontal tubes. J. Heat Transfer 120, 193–213.
Graham, D., Chato, J.C., Newell, T.A., 1999. Heat transfer and pressure drop during condensation of refrigerant 134a in an axially grooved tube. Int. J. Heat Mass Transfer 42, 1935–1944.
Kalman, H., Mori, Y.H., 2002. Experimental analysis of a single vapor bubble condensing in subcooled liquid. Chem. Eng. J. 85, 197–206.
Larson, R.G., Morrow, N.R., 1981. Effects of sample size on capillary pressures in porous media. Powder Technol. 30, 123–138.
Lips, S., Meyer, J.P., 2011. Two-phase flow in inclined tubes with specific reference to condensation: a review. Int. J. Multiphase Flow 37, 845–859.
Lips, S., Meyer, J.P., 2012. Experimental study of convective condensation in an inclined smooth tube. Part I: inclination effect on flow pattern and heat transfer coefficient. Int. J. Heat Mass Transfer 55, 395–404.
Mandhane, J.M., Gregory, G.A., Aziz, K., 1974. A flow-pattern map for gas–liquid flow in horizontal pipes. Int. J. Multiphase Flow 1, 537–553.
Miyara, A., Otsubo, Y., 2002. Condensation heat transfer of herringbone micro fin tubes. Int. J. Therm. Sci. 41, 639–645.
Suriyan, L., Somchai, W., 2010. The effects of corrugation pitch on the condensation heat transfer coefficient and pressure drop of R134a inside horizontal corrugated tube. Int. J. Heat Mass Transfer 53, 2924–2931.
Tsai, J.H., Lin, L.W., 2002. Active micro-fluidic mixer and gas bubble filter driven by thermal bubble micro-pump. Sens. Actuators 97–98, 665–671.
Vasil'ev, A.P., 2003. Dynamics and heat transfer in collapse of a bubble containing wet vapor in hydrophobic liquid. J. Eng. Phys. Thermophys. 76, 838–846.
Xu, J.L., Zhang, X.M., 2005. Start-up and steady thermal oscillation of a pulsating heat pipe. Heat Mass Transfer 41, 685–694.